Resonance Clustering in Wave Turbulent Regimes: Integrable Dynamics

Miguel D. Bustamante[1] and Elena Kartashova[2,*]

[1] *School of Mathematical Sciences, University College Dublin, Belfield,*
Dublin 4, Ireland.
[2] *IFA, J. Kepler University, Linz 4040, Austria.*

Abstract. Two fundamental facts of the modern wave turbulence theory are 1) existence of power energy spectra in k-space, and 2) existence of "gaps" in this spectra corresponding to the resonance clustering. Accordingly, three wave turbulent regimes are singled out: *kinetic*, described by wave kinetic equations and power energy spectra; *discrete*, characterized by resonance clustering; and *mesoscopic*, where both types of wave field time evolution coexist. In this review paper we present the results on integrable dynamics of resonance clusters appearing in discrete and mesoscopic wave turbulent regimes. Using a novel method based on the notion of dynamical invariant we show that some of the frequently met clusters are integrable in quadratures for arbitrary initial conditions and some others-only for particular initial conditions. We also identify chaotic behaviour in some cases. Physical implications of the results obtained are discussed.

PACS: 47.10.Df, 47.10.Fg, 02.70.Dh

Key words: Resonance clustering, Hamiltonian formulation, wave turbulent regimes, NR-diagram, integrable dynamics.

1 Introduction

The broad structure of modern nonlinear science born at the edge of physics and mathematics includes an enormous number of applications in cosmology, biochemistry, electronics, optics, hydrodynamics, economics, neuroscience, etc. The emergence of nonlinear science itself as a collective interdisciplinary activity is due to the awareness that

Corresponding author. Email addresses: `miguel.bustamante@ucd.ie` (M. D. Bustamante),
`elena.kartaschova@jku.at` (E. Kartashova)

its dynamic concepts first observed and understood in one field (for example, population biology, flame-front propagation, non-linear optics or planetary motion) could be useful in others (such as in chemical dynamics, neuroscience, plasma confinement or weather prediction). The theory of integrable Hamiltonian systems, a generalization of the classical theory of differential equations, is the fundamental part of the whole nonlinear science for it yields good mathematical models for many physical phenomena. Various classifications of integrable systems are presently known which turned out to be quite useful for physical applications. Classifications are known based on the various intrinsic properties of integrable systems [56]: symmetries, conservation laws, Lax-pairs, etc. In [3] the general classification of integrable Hamiltonian systems is presented based on the form of their topological invariants. The usefulness of this classification is demonstrated in several problems on solid mechanics. In particular, it is proven that two famous problems-the Euler case in rigid body dynamics and the Jacobi problem of geodesics on the ellipsoid-are orbitally equivalent. In [12] the idea of classification is presented based on normal forms of a certain class of bi-hamiltonian PDEs. Miscellaneous hierarchies of integrable PDEs are presented in [50].

The list can be prolonged further but the main point for us presently is the following: the notion of integrability itself is ambitious! There are many quite different definitions of integrability, for instance integrability in terms of elementary functions (equation $\ddot{y} = -y$ has the explicit solution $y = a\sin(x+b)$); integrability *modulo* class of functions (equation $\ddot{y} = f(y)$ has general solutions in terms of elliptic functions), etc. An example of less obvious definition of integrability is C-integrability, first introduced in [6]: integrability *modulo* change of variables, meaning that a *nonlinear* equation is called C-integrable if it can be turned into a *linear* equation by an appropriate invertible change of variables. For instance, Thomas equation $\psi_{xy} + \alpha\psi_x + \beta\psi_y + \psi_x\psi_y = 0$ is C-integrable. Profound discussion on the subject can be found in [36]. In the present paper, integrability is interpreted in terms of the existence of a number of independent dynamical invariants of the system; for each in-this-sense-integrable system, solutions are then written out *in quadratures*.

The dynamical systems we are interested in, describe nonlinear resonance clusters appearing in evolutionary dispersive wave systems in two space variables. Nonlinear resonances are ubiquitous in physics. They appear in a great amount of typical mechanical systems [13,38], in engineering [8,18,39,63], astronomy [55], biology [16], etc. Euler equations, regarded with various boundary conditions and specific values of some parameters, describe an enormous number of nonlinear dispersive wave systems (capillary waves, surface water waves, atmospheric planetary waves, drift waves in plasma, etc) all possessing nonlinear resonances.

The classical approach of statistical wave turbulence theory in a nonlinear wave system assumes weak nonlinearity, randomness of phases, infinite-box limit, existence of an inertial interval in wavenumber space (k_0,k_1) (where energy input and dissipation are separated in scales from both energy input and dissipation area) as well as some other assumptions omitted here (see [70] for more details). As a result, the wave system is energy conserving, and wave kinetic equations describing the wave spectrum have sta-

Layers	Acting elements	Observables		Regimes
discrete	exact and quasi-resonances	distinct modes, coherent phases, infinite k-space		*discrete*
				mesoscopic
continuous	non-resonant (or approximate) interactions	KZ-spectra, stochastic phases, finite inertial interval in k-space		*kinetic*
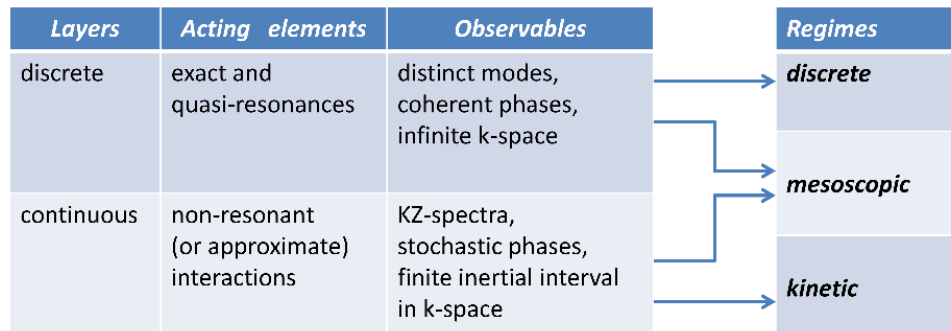
Figure 1: Color online. Schematic representation of wave turbulent regimes.

tionary solutions in the form of Kolmogorov-Zakharov (KZ) energy power spectra $k^{-\alpha}$, $\alpha > 0$ (see [59,70,73], etc).

As it was first established in the frame of the model of laminated turbulence, [24], KZ-spectra have "gaps" formed by exact and quasi-resonances (that is, resonances with small enough resonance broadening). This yields two distinct layers of turbulence in an arbitrary nonlinear wave system-continuous and discrete-and their interplay generates three possible wave turbulent regimes: *kinetic*, *discrete* and *mesoscopic* as it is shown in Fig. 1.

The very concept of the *mesoscopic regime* has been introduced in [74] and its existence has been demonstrated in numerical simulations with dynamical equations for surface gravity waves. In this paper, *frozen turbulence*-characterized by the existence of "frozen" (or non-interacting) modes keeping their energy and taking no part in the energy transfer over *k*-spectrum at some time-scale-is regarded as an opposite case to the kinetic regime. Example of frozen turbulence (for capillary waves) is given in [62] where also the notion of frozen turbulence was originally presented. Frozen turbulence is one possible realization of a *discrete regime* first introduced in [27].

Discrete regime is characterized by the behavior of *distinct modes*, whether frozen or taking part in exact and quasi-resonances. The existence of non-interacting modes for various 3-wave resonance systems has been proven analytically in [21]; in particular, it was shown that capillary waves with dispersion function $\omega \sim k^{3/2}$ have no exact 3-wave resonances in bounded domains and therefore all modes will be frozen (at the corresponding time scale and for appropriate energies, this will be explicated below in the present Section). Example of a wave system where both types of modes do exist (atmospheric planetary waves) is given in [22]: both interacting and frozen modes have been observed (see [22], Fig. 1 and Fig. 3 correspondingly). Examples of discrete regimes for capillary waves in various media and for different forms of laboratory tanks can be found in [10].

These theoretical findings are confirmed by numerous laboratory experiments. For instance, in the experiments with gravity surface wave turbulence in a laboratory flume, [11],

only a discrete regime has been identified while in [69] coexistence of both types of time evolution has been established. Taking into account additional physical parameters in a wave system transition from kinetic to mesoscopic regime can be observed as it was demonstrated in [9] for capillary water waves, with and without rotation.

It is important to realize that for any of these regimes to be observable, a small parameter, $0 < \varepsilon \ll 1$, should be introduced, i.e., we always regard weakly nonlinear case yielding small enough energies of wave systems under consideration. There are various ways of introducing a small parameter: for instance, for planetary waves the ratio of the particle velocity to the phase velocity is usually taken as the small parameter; for various water waves it can be taken as the steepness of the waves; etc. Accordingly, in all dynamical systems studied further on, the modes' amplitudes depend on the "slow" time, εt, and are usually refereed to as slowly changing amplitudes; time scale t corresponds to the linear case and is sometimes called "fast" time.

From a mathematical point of view, the very special role of resonant solutions has been first demonstrated by Poincaré who proved, using Calogero's terminology, that a nonlinear ODE is C-integrable if it has no resonance solutions (see [2] and references therein). This statement allows the following Hamiltonian formulation [70]:

$$i\dot{a}_{\mathbf{k}} = \frac{\partial \mathcal{H}}{\partial a_{\mathbf{k}}^*}, \tag{1.1}$$

where $a_{\mathbf{k}}$ is the amplitude of the Fourier mode corresponding to the wavevector $\mathbf{k}$ and the Hamiltonian $\mathcal{H}$ is represented as an expansion in powers $\mathcal{H}_j$ which are proportional to the product of j amplitudes $a_{\mathbf{k}}$:

$$\mathcal{H} = \mathcal{H}_2 + \mathcal{H}_3 + \mathcal{H}_4 + \cdots,$$

$$\mathcal{H}_2 = \sum_{n=1}^{\infty} \omega_{\mathbf{k}} |a_{\mathbf{k}}|^2,$$

$$\mathcal{H}_3 = \sum_{\mathbf{k_1}, \mathbf{k_2}, \mathbf{k_3}} V_{12}^3 a_1^* a_2 a_3 \delta_{12}^3 + \text{complex conj.,}$$

$$\mathcal{H}_4 = \sum_{\mathbf{k_1}, \mathbf{k_2}, \mathbf{k_3}, \mathbf{k_4}} T_{34}^{12} a_1^* a_2^* a_3 a_4 \delta_{34}^{12} + \text{complex conj.,} \cdots.$$

Here for brevity we introduced the notation $a_j \equiv a_{\mathbf{k}_j}$ while $\delta_{12}^3 \equiv \delta(\mathbf{k_3} - \mathbf{k_1} - \mathbf{k_2})$ and $\delta_{34}^{12} \equiv \delta(\mathbf{k_3} + \mathbf{k_4} - \mathbf{k_1} - \mathbf{k_2})$ are the Kronecker symbols for 3- and 4-wave interactions accordingly. It follows from (1.1) that quadratic Hamiltonian produces a linear equation of motion, $i da_{\mathbf{k}} / dt = \omega_{\mathbf{k}} a_{\mathbf{k}}$, while nonlinear contribution is given by the terms $\mathcal{H}_3, \mathcal{H}_4$ and so on. If $\mathcal{H}_3 \neq 0$, three-wave resonant processes are dominant (see [28] for more details). These satisfy the resonance conditions:

$$\begin{cases} \omega(\mathbf{k}_1) + \omega(\mathbf{k}_2) - \omega(\mathbf{k}_3) = 0, \\ \mathbf{k}_1 + \mathbf{k}_2 - \mathbf{k}_3 = 0, \end{cases} \tag{1.2}$$

where $\omega(\mathbf{k})$ is a dispersion relation for the linear wave frequency. Further on, the notation ω_k is used for $\omega(\mathbf{k})$. The corresponding dynamical system has a general form

$$i\dot{B}_{\mathbf{k}} = \sum_{\mathbf{k_1},\mathbf{k_2}} \left(V_{12}^{\mathbf{k}} B_1 B_2 \delta_{12}^{\mathbf{k}} + 2V_{\mathbf{k}2}^{1*} B_1 B_2^* \delta_{\mathbf{k}3}^{1} \right) \tag{1.3}$$

(notations B_j are used further on for the slowly changing amplitudes of resonant modes). If $\mathcal{H}_3 = 0$, four-wave resonances have to be studied, and so on. To confirm that $\mathcal{H}_3 \neq 0$ and three-wave resonances are dominant, one has to find solutions of (1.2) and check that $V_{12}^3 \neq 0$ at least at some resonant triads. Afterwards the corresponding dynamical system has to be studied.

Notice that if some non-zero resonance width Δ is taken into account,

$$\omega(\mathbf{k}_1) + \omega(\mathbf{k}_2) - \omega(\mathbf{k}_3) = \Delta, \qquad \Delta > 0, \tag{1.4}$$

it can be regarded as a shift in resonant wave frequencies, Δ_{B_k}, which causes resonance broadening, [61, 64, 74], etc. Broadening in a three-wave system is characterized by the interrelation between Δ_{B_k} and inverse nonlinear oscillation time τ_k^{-1} of resonant modes,

$$\tau_k^{-1} \approx |V_{12}^3 B_k|. \tag{1.5}$$

Accordingly, kinetic regime corresponds to

$$|\Delta_{B_k}| \gg \tau_k^{-1}, \tag{1.6}$$

discrete regime corresponds to

$$|\Delta_{B_k}| \ll \tau_k^{-1}, \tag{1.7}$$

while mesoscopic regime corresponds to

$$|\Delta_{B_k}| \simeq \tau_k^{-1}. \tag{1.8}$$

In discrete regime phases of individual modes are coherent; however if the width $|\Delta_{B_k}|$ is substantially larger that τ_k^{-1}, the coherence is lost, which is a necessary condition for the kinetic regime to occur. This means that in a 3-wave system possessing resonances, resonance clustering plays major or substantial role (discrete and mesoscopic regimes correspondingly), while in kinetic regime statistical description should be used. The fact that generation of kinetic regime occurs *via* spectral broadening of discrete harmonics has been demonstrated experimentally in [61] (capillary water waves).

It has been first proven in [23] that for a big class of physically relevant dispersion functions ω, the set of all wavevectors satisfying (1.2) can be divided into non-intersecting classes and solutions of (1.2) can be looked for in each class separately; the results keep true for some non-zero resonance width $\Delta > 0$. The method of q-class decomposition first introduced in [25] has been developed specially for solving systems of the form (1.2) in

integers; details of its implementation for various rational and irrational dispersion functions are given in [29–31]. General description of the q-class method and corresponding programming codes are given in [28], in Section 3 and Appendix correspondingly.

An immediate consequence of the q-class method is that dynamical system (1.3) can be reduced to *a few dynamical systems* of smaller order, and each of these smaller dynamical systems can be investigated independently from all others. In [34], construction of a set of reduced dynamical systems corresponding to the solutions of (1.2) and the systems themselves are given explicitly (as an example, resonances of oceanic planetary waves were considered in the spectral domain $0 \leq m, n \leq 50$). The integrability of the dynamical system for an isolated triad is well known (see e.g., [68]) while integrability of some resonance clusters has been studied in [4, 48, 49, 66, 67], etc.

The main goal of the present review is to study systematically the integrable dynamics of the most frequently met resonance clusters. We begin with a brief introduction of NR-diagrams (NR for nonlinear resonance) which give a handy graphical representation of a generic resonance cluster and allow us to recover uniquely the dynamical system corresponding to each cluster [28].

2   NR-diagrams

In systems with cubic Hamiltonian, a resonant triad is called *primary cluster* (a resonant quartet is a primary cluster in a system with quadric Hamiltonian, and so on). All other clusters (formed by a few primary clusters connected via one of a few joint modes) are called *generic* clusters or simply clusters. The dynamical system for a complex triad in the standard Manley-Rowe form reads

$$\dot{B}_1 = ZB_2^* B_3, \qquad \dot{B}_2 = ZB_1^* B_3, \qquad \dot{B}_3 = -ZB_1 B_2, \tag{2.1}$$

and is known to be integrable, with two conservation laws in the Manley-Rowe form being

$$I_{23} = |B_2|^2 + |B_3|^2, \qquad I_{13} = |B_1|^2 + |B_3|^2 \tag{2.2}$$

(notations B_j are used for the amplitudes of resonantly interacting waves forming a triad).

Due to the criterion of nonlinear instability for a triad [17], the mode with maximal frequency, ω_3, is unstable while the modes ω_1 and ω_2 are neutral. This means that the form of dynamical systems and accordingly time evolution of the modes belonging to a generic cluster depends crucially on the fact whether joint modes within a cluster are stable or unstable. With the purpose to distinguish between these cases, the notations A-mode (active) and P-mode (passive) are introduced for ω_3-mode and ω_1- and ω_2-modes respectively, [33]. This allows to describe all possible connection types within a generic cluster. For instance, 1-mode connection of two triads can be of AA-, AP- and PP-type; 1-mode connection of three triads can be of AAA-, AAP-, APP-type and PPP-type, 2-mode

connection between two triads can be of AA-PP-, AP-AP-, AP-PP- and PP-PP-types, and so on.

In the topological representation [34] of the solution set of (1.2) this dynamical information has been kept implicit, as part of a programming code used to construct dynamical system, while each triad within a cluster was shown as an unmarked triangle (see Fig. 2).

More compact graphical representation of a resonance cluster is given by its NR-diagram, [27]. In a NR-diagram each vertex represents not a resonant mode but a *primary cluster*, that is, a triad and a quartet in a three- and four-wave system correspondingly. A NR-diagram in systems with cubic Hamiltonian consists of following building elements- a triangle and two types of half-edges, bold for A-mode and dotted for P-mode. It can be proven (see [28], Section 3) that in this case the form of NR-diagram defines *uniquely* corresponding dynamical system. Examples of NR-diagrams for some resonance clusters shown in Fig. 2 are displayed in Fig. 3. Below, examples of dynamical systems are given for two generic clusters shown in Fig. 2:

1. Cluster consisting of two triads a and b, whose connecting mode is active in one triad and passive in the other triad, say $B_{3a} = B_{1b}$. In other words, a cluster with one AP-connection. It is called AP-butterfly [33] and its dynamical system is

$$\begin{cases} \dot{B}_{1a} = Z_a B_{2a}^* B_{3a}, & \dot{B}_{2a} = Z_a B_{1a}^* B_{3a}, & \dot{B}_{3a} = -Z_a B_{1a} B_{2a} + Z_b B_{2b}^* B_{3b}, \\ \dot{B}_{2b} = Z_b B_{3a}^* B_{3b}, & \dot{B}_{3b} = -Z_b B_{3a} B_{2b}. \end{cases} \tag{2.3}$$

2. Cluster consisting of three triads a, b and c, with one AA- and one PP-connections, say, $B_{3a} = B_{3b}$ and $B_{1b} = B_{1c}$. The dynamical system reads

$$\begin{cases} \dot{B}_{1a} = Z_a B_{2a}^* B_{3a}, & \dot{B}_{2a} = Z_a B_{1a}^* B_{3a}, & \dot{B}_{3a} = -Z_a B_{1a} B_{2a} - Z_b B_{1b} B_{2b}, \\ \dot{B}_{1b} = Z_b B_{2b}^* B_{3a} + Z B_{2c}^* B_{3c}, & \dot{B}_{2b} = Z_b B_{1b}^* B_{3a}, \\ \dot{B}_{2c} = Z_c B_{1b}^* B_{3c}, & \dot{B}_{3c} = -Z_c B_{1b} B_{2c}. \end{cases} \tag{2.4}$$

The Manley-Rowe constants can be written out immediately for each of these systems, being combinations of corresponding constants for each triad. For instance, for (2.3) they have the form

$$I_{12b} = |B_{1b}|^2 - |B_{2b}|^2, \quad I_{23b} = |B_{2b}|^2 + |B_{3b}|^2, \quad I_{ab} = |B_{1b}|^2 + |B_{3a}|^2 + |B_{3b}|^2. \tag{2.5}$$

The main difference between NR-diagram and statistical Wyld diagrams (originating from Keldysh's technique for non-equilibrium processes which in its turn is an offspring of Feynman diagram) used in wave turbulence theory can be formulated as follows. Each Wyld diagram corresponds to one term in the asymptotic expansion and *does not allow to compute the amplitudes* of the scattering process. On the other hand, a set of NR-diagram describes completely all resonance clusters in a wave system and allows to write out *explicit form of the dynamical system on the modes' amplitudes* for each cluster.
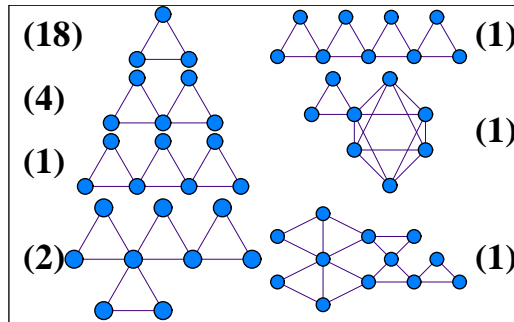
Figure 2: Topological structure of the cluster set for the oceanic planetary waves, $\omega \sim 1/\sqrt{m^2+n^2}$, in the domain $m,n \le 50$. 7 types of resonance clusters have been found, the number of the clusters of each type is shown in parenthesis. Figure is taken from [34].
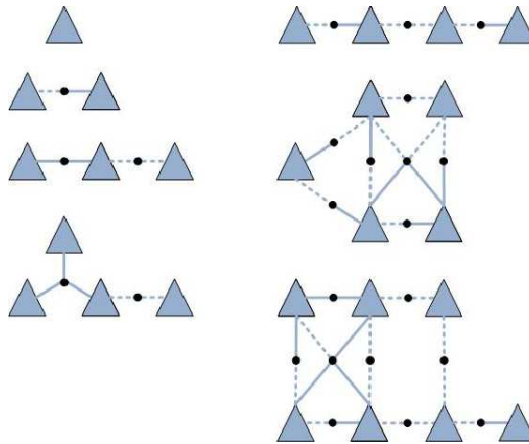
Figure 3: NR-diagrams for some resonance clusters shown in Fig. 2.

This means that the two techniques are not mutually exclusive and either this or that should be applied to a particular regime in a wave turbulent system. Rather, these two diagram's types are complementary: Wyld diagrams visualize kinetic regime properties while NR-diagrams-discrete regime properties.

In mesoscopic regime appearing clusters can be fairly big and consist of a few hundreds or even thousands of connected triads. For instance, in [42] resonance clustering of 2-dimensional atmospheric planetary waves in the spectral domain with wave numbers ≤ 1000 is studied; in this case the maximal cluster consists of about 4000 triads. However, 82,2%% of all clusters are isolated triads and 10.5%% are two-triad clusters, i.e., dynamics of the majority of clusters can be investigated by the methods presented below.

As it will be shown below, connection types within a cluster define indeed the integrability of the corresponding dynamical systems. In order to demonstrate it we will use the notion of dynamical invariant first introduced in [4] which is given in the next section and illustrated by the example of harmonic oscillator.

3 Dynamical invariants

3.1 Definition

From here on, general notations and terminology will follow Olver's book [56] and Einstein convention on repeated indices and $f_{,i} \equiv \partial f / \partial x^i$. Consider a general N-dimensional system of autonomous evolution equations of the form:

$$\frac{dx^i}{dt}(t) = \Delta^i(x^j(t)), \qquad i = 1, \cdots, N. \tag{3.1}$$

Any scalar function $f(x^i, t)$ that satisfies

$$\frac{d}{dt}(f(x^i(t), t)) = \frac{\partial}{\partial t}f + \Delta^i f_{,i} = 0$$

is called *a conservation law* in [56]. It is easy to see that this definition gives us two types of conservation laws: (i) those of the form $f(x^i)$ (no explicit time-dependence), and (ii) those of the form $f(x^i, t)$, where the time dependence is explicit. The first type determines an invariant manifold for the dynamical system (3.1) (*time-independent* conservation law) and the second type constrains the time evolution of the system within the invariant manifold(s) (*time-dependent* conservation law). To keep in mind the difference between these two types of conservation laws, we call the first type just a conservation law (CL), and the second type-a *dynamical invariant*.

We are interested in determining the solution $x^i(t)$, $i = 1, \cdots, N$, of a given dynamical system of the form (3.1). One possible way to do that is by finding N functionally independent dynamical invariants for the system (3.1). This is equivalent to finding $(N-1)$ functionally independent conservation laws and *one* dynamical invariant (the equivalence can be proven, for example, using the implicit function theorem).

As it was shown in [5], in some cases the knowledge of only $(N-2)$ functionally independent CLs is enough for constructing explicitly: (i) a new CL functionally independent of the others, and (ii) a corresponding dynamical invariant, determining the solution $x^i(t)$, $i = 1, \cdots, N$. This follows from the Theorem on $(N-2)$-integrability [5], whose formulation is given below for the readers' convenience.

Theorem 3.1. (Theorem on $(N-2)$-integrability) *Let us assume that the system* (3.1) *possesses a standard Liouville volume density*

$$\rho(x^i): (\rho\Delta^i)_{,i} = 0,$$

and $(N-2)$ functionally independent CLs, $H^1, \cdots, H^{N-2}$. Then a new CL in quadratures can be constructed, which is functionally independent of the original ones, and therefore the system is integrable.

3.2 Example: damped harmonic oscillator

3.2.1 Dynamical invariants, CLs and solutions

To illustrate the complementarity of conserved laws and dynamical invariants, we present an illustrative example from mechanics for the case $N=2$. Consider the damped harmonic oscillator. The equations of motion in non-dimensional form can be written as:

$$\dot{q}=p, \qquad \dot{p}=-q-\alpha p, \tag{3.2}$$

where $\alpha \geq 0$ is the damping coefficient. This is a dynamical system of the form (3.1) with $N=2$. Now we want to fully determine the solution of the dynamical system (3.2). For this we need to know both a CL and a dynamical invariant. Indeed, let us consider separately the cases $\alpha=0$ (harmonic oscillator) and $0<\alpha<2$ (sub-critically damped harmonic oscillator).

1. Case $\alpha=0$. We have the CL

$$E(q,p)=\frac{1}{2}(p^2+q^2) \tag{3.3}$$

(energy) and the dynamical invariant

$$T(q,p,t)=t-\arctan\left(\frac{q}{p}\right). \tag{3.4}$$

Since

$$\frac{d}{dt}\left(E(q(t),p(t))\right)=0, \qquad \frac{d}{dt}\left(T(q(t),p(t),t)\right)=0,$$

then we have

$$E(q(t),p(t))=E_0, \qquad T(q(t),p(t),t)=T_0,$$

constants depending on the initial conditions $q(0),p(0)$. This information is enough to find the solution $q(t),p(t)$ of the system:

$$q(t)=\sqrt{2E_0}\sin(t-T_0), \qquad p(t)=\sqrt{2E_0}\cos(t-T_0), \tag{3.5}$$

which can be checked by direct substitution in (3.2).

In Fig. 4, we show level surface of conservation law $E=30$ (Fig. 4(a)), level surface of dynamical invariant $T=0$ (Fig. 4(b)) and solution trajectory $q(t),p(t)$ (Fig. 4(c)). This solution is actually the intersection of the level surfaces $E=30$ and $T=0$; for completeness of presentation, we show together the level surfaces and the solution in Fig. 5 (left panel).

Notice that coordinates q,p are not suitable for a global parametrization of dynamical invariant T, (3.4), because $\arctan(x)$ is multi-valued. This problem can easily be overcome by using new coordinates (R,θ):

$$q=R\sin\theta, \qquad p=R\cos\theta \tag{3.6}$$
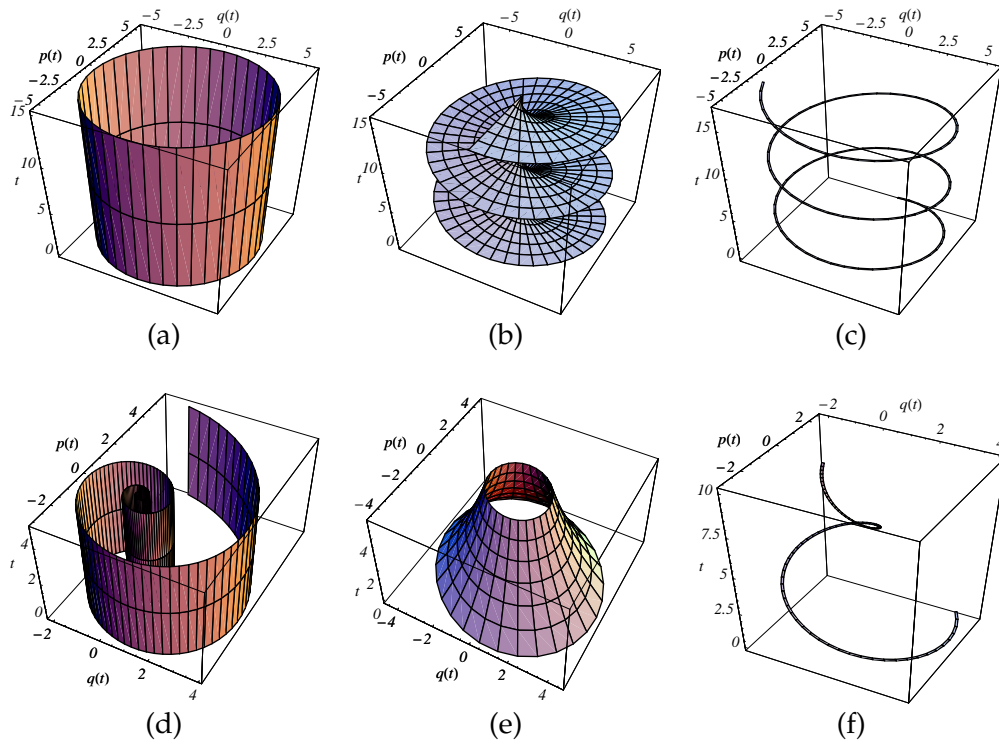
Figure 4: Color online. Harmonic oscillator (case $\alpha=0$): (a): a level surface of conservation law $E(q,p)=30$, Eq. (3.3); (b): a level surface of dynamical invariant $T(q,p,t)=0$, Eq. (3.7); (c): solution trajectory $(q(t),p(t))$, Eq. (3.5), corresponding to $E=30$, $T=0$. Sub-critically damped harmonic oscillator (case $0<\alpha<2$): (d): a level surface of conservation law $C(q,p)=30$, Eq. (3.11); (e): a level surface of dynamical invariant $D(q,p,t)=20$, Eq. (3.8); (f): solution trajectory $(q(t),p(t))$, Eq. (3.12), corresponding to $C=30$, $D=20$.
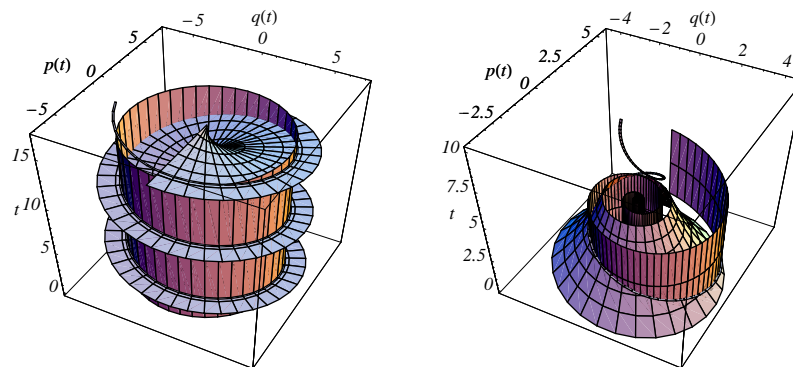
Figure 5: Color online. Left panel: harmonic oscillator (case $\alpha=0$): combined plot of level surface of conservation law $E(q,p)$, level surface of dynamical invariant $T(q,p,t)$ and solution trajectory $(q(t),p(t))$. Notice the general property that the intersection of the level surfaces of E and T *is* the solution trajectory. Right panel: sub-critically damped harmonic oscillator (case $0<\alpha<2$): combined plot of level surface of conservation law $C(q,p)$, level surface of dynamical invariant $D(q,p,t)$ and solution trajectory $(q(t),p(t))$. Notice the general property that the intersection of the level surfaces of C and D *is* the solution trajectory.

which allow us to rewrite T as

$$T(q,p,t) = \widetilde{T}(R,\theta,t) = t - \theta, \tag{3.7}$$

thereby eliminating the ambiguity. The plot of level surface $\widetilde{T} = 0$ in the upper middle panel of Fig. 4 was done using the parameters (R,t).

2. Case $0 < \alpha < 2$. Let $\alpha/2 = \sin\varphi$, then a dynamical invariant for the system is known:

$$D(q,p,t) = (p^2 + q^2 + 2pq\sin\varphi)\exp[2t\sin\varphi]. \tag{3.8}$$

We need to find a CL in order to determine the solution. Here we simply state the following CL:

$$C(q,p) = \frac{\cos\varphi}{2}(p^2 + q^2 + 2pq\sin\varphi) \times \exp\left[2\tan\varphi\arctan\left(\frac{q}{p}\sec\varphi + \tan\varphi\right)\right]. \tag{3.9}$$

The method of construction of this CL is not important right now, it will be detailed in the next section. In Fig. 4, we show level surface of conservation law $C = 30$ (Fig. 4(d)), level surface of dynamical invariant $D = 20$ (Fig. 4(3)) and solution trajectory $q(t), p(t)$ (Fig. 4(f)). This solution corresponds to the intersection of the level surfaces $C = 30$ and $D = 20$; for completeness, the level surfaces and the solution are shown together in Fig. 5 (right panel).

Similar to the case of $\alpha = 0$ dynamical invariant, the CL $C(q,p)$ is not globally defined. The following change of variables is needed:

$$q = R\sec\varphi\sin(\theta - \varphi), \qquad p = R\cos\theta\sec\varphi, \tag{3.10}$$

in order to parameterize globally the CL. The result is

$$C(q,p) = \widetilde{C}(R,\theta) = \frac{\cos\varphi}{2}R^2\exp[2\theta\tan\varphi]. \tag{3.11}$$

It is important to realize that the two changes of variables (3.6) and (3.10) are suggested by the form of the respective invariants. Moreover, in the new variables (R,θ), both T and C take a simpler form (see (3.7) and (3.11)). The reason for it is clear in the case $\alpha = 0$ because (R,θ) are the well-known action-angle variables. In the general case, the variables (R,θ) determine a covering of the original variables.

The solution of the dynamical system is finally

$$q(t) = \sqrt{D}\sin\left(t\cos\varphi + \frac{1}{2}\log\left(\frac{C}{D}\right)\cot\varphi - \varphi\right)(\cos\varphi\exp[t\sin\varphi])^{-1}, \tag{3.12a}$$

$$p(t) = \sqrt{D}\cos\left(t\cos\varphi + \frac{1}{2}\log\left(\frac{C}{D}\right)\cot\varphi\right)(\cos\varphi\exp[t\sin\varphi])^{-1}. \tag{3.12b}$$

3.2.2   Construction of conservation law

To illustrate the procedure of construction of a conservation law, we take as an example the sub-critically damped harmonic oscillator, i.e., Eq. (3.2) with $0 < \alpha < 2$. Here $N = 2$ and $\Delta^1 = p$, $\Delta^2 = -q - \alpha p$. The dynamical system is just 2-dimensional and we will write it as a vector $(\Delta^1, \Delta^2)^T$. The Theorem requires the existence of a standard Liouville volume density $\rho(x^1, x^2)$ satisfying

$$(\rho \Delta^1)_{,1} + (\rho \Delta^2)_{,2} = 0, \tag{3.13}$$

and does not require the knowledge of conservation laws. In general, a Liouville density, solution of (3.13), is interpreted as follows. A small region $\mathcal{R}(t)$ with a volume $V(t)$ in phase space (x_1, x_2), will evolve in time due to the dynamical system (3.2). Then, ρ is defined in such a way that the product $\rho V(t)$ is conserved in time as $\mathcal{R}(t)$ evolves. For the harmonic oscillator, it is well known that the volume of $\mathcal{R}(t)$ is preserved, i.e., a constant function is a Liouville density. For the damped harmonic oscillator, a direct check shows that a Liouville density is $\rho(q, p) = (q^2 + p^2 + 2\alpha q p)^{-1}$. With this information we just need to solve (3.14) for H:

$$\begin{pmatrix} 0 & 1 \\ -1 & 0 \end{pmatrix} \begin{pmatrix} H_{,1} \\ H_{,2} \end{pmatrix} = \begin{pmatrix} \rho \Delta^1 \\ \rho \Delta^2 \end{pmatrix}. \tag{3.14}$$

The answer can be obtained by direct integration (see [4] for more details):

$$H(q, p) = -\left(\frac{q \alpha \arctan\left(\frac{2p + q\alpha}{\sqrt{-(q^2(-4 + \alpha^2))}} \right)}{\sqrt{-(q^2(-4 + \alpha^2))}} \right) + \frac{\log(p^2 + q^2 + pq\alpha)}{2}. \tag{3.15}$$

The conservation law $C(q, p)$ given by Eq. (3.9) is a function of H, chosen for its nice form:

$$C = \frac{\cos \varphi}{2} \exp(2H).$$

4   Triad

As it was shown above, the notion of dynamical invariant is an important tool for constructing new physically relevant conservation laws that can afterwards be studied in a simple laboratory experiment. In this section we would like to use this approach to prove integrability of a complex triad with dynamical system (2.1). Though integrability of (2.1) is a well-known fact, the explicit solution of (2.1) is usually written for a particular case, namely, when the dynamical phase-a phase combination corresponding to the chosen resonance conditions-is either zero or constant (see [41], pp.132, Eq. (6.7) and [58], pp.156, Eq. (3.26.19), etc). Accordingly, till recently all known analytical solutions of the dynamical equations for a triad has been obtained for this *particular case of initial conditions*.

On the other hand, it is well known that dynamical phases play a substantial role in the dynamics of resonant clusters, e.g., [65], and their effect can easily be observed in numerical simulations [5]. This was our motivation for constructing first an explicit solution in the amplitude-phase presentation, with *generic initial conditions*. Another important point is that an elastic pendulum with suitably chosen parameters can be used as a mechanical model of a resonant triad, and the results can be applied for the description of large-scale motions in the Earth's atmosphere, e.g., [44]. In fact, this simple mechanical model can be used for a laboratory study of dynamical characteristics of primary clusters in an *arbitrary* system with cubic Hamiltonian.

4.1 Integrability

In this case the system can be reduced to $N = 4$ (see [4] for more details), the Theorem on $(N-2)$-integrability can be applied and we obtain the following CL:

$$H_T = \text{Im}(B_1 B_2 B_3^*), \tag{4.1}$$

which is the canonical Hamiltonian for this case and can, of course, be written out directly. A dynamical invariant for this system was originally presented in [4], in terms of the three real roots $R_1 < R_2 < R_3$ of the cubic polynomial

$$x^3 + x^2 = \frac{2}{27} - \left(27 H_T^2 - (I_{13} + I_{23})(I_{13} - 2I_{23})(I_{23} - 2I_{13})\right) \left[27(I_{13}^2 - I_{13}I_{23} + I_{23}^2)^{\frac{3}{2}}\right]^{-1},$$

but these roots' dependence on the coordinates or the CLs was not made explicit. Moreover, the explicit solution for the amplitudes C_j and phases θ_j in the amplitude-phase representation

$$B_j = C_j \exp(i\theta_j),$$

was not provided. Here we improve the form of dynamical invariant and also produce explicit and useful expressions for the full solution, based on the trigonometric representation of the three real roots in the so-called *Casus Irreducibilis*.

4.2 Amplitude-phase representation

System (2.1) in the standard amplitude-phase representation $B_j = C_j \exp(i\theta_j)$ reads:

$$\begin{cases} \dot{C}_1 = ZC_2C_3\cos\varphi, & \dot{C}_2 = ZC_1C_3\cos\varphi, \\ \dot{C}_3 = -ZC_1C_2\cos\varphi, & \dot{\varphi} = -ZH_T(C_1^{-2} + C_2^{-2} - C_3^{-2}), \end{cases} \tag{4.2}$$

where $\varphi = \theta_1 + \theta_2 - \theta_3$ is the dynamical phase. The conservation laws (2.2) do not change their form in the new variables: $I_{23} = C_2^2 + C_3^2$, $I_{13} = C_1^2 + C_3^2$, but the Hamiltonian H_T reads now $H_T = C_1 C_2 C_3 \sin\varphi$. Let us introduce new variables:

$$\rho = \frac{I_{23}}{I_{13}} \tag{4.3}$$

and $\alpha \in [0,\pi]$ defined by

$$\cos\alpha = \frac{\left(-2+3\rho+3\rho^2-2\rho^3\right)I_{13}{}^3-27H_T{}^2}{2\left(1-\rho+\rho^2\right)^{\frac{3}{2}}I_{13}{}^3}. \tag{4.4}$$

Notice that $|\cos\alpha| \le 1$ for dynamically accessible system's configurations. Indeed, the use of intermediate variables

$$p = 2\left(1-\rho+\rho^2\right)^{\frac{3}{2}} \quad \text{and} \quad q = -2+3\rho+3\rho^2-2\rho^3,$$

allows one to conclude immediately that $p \ge 0$ and $p \ge |q|$, $\forall\rho$. Both inequalities become equalities if $\rho=0$ or $\rho=1$. This yields

$$\left(H_T^2\right)_{\max} = \left(\frac{I_{13}}{3}\right)^3 (p+q) \ge 0, \quad \text{for} \quad \cos\alpha = -1,$$

and $(\cos\alpha)_{\max} = q/p \le 1$, for $H_T = 0$, where $(H_T^2)_{\max}$ and $(\cos\alpha)_{\max}$ are maximum values of H_T^2 and $\cos\alpha$ correspondingly.

Now, the solution of (4.2) is obtained in terms of Jacobian functions with modulus

$$\mu = \cos\left(\frac{\alpha}{3}+\frac{\pi}{6}\right)\left[\cos\left(\frac{\alpha}{3}-\frac{\pi}{6}\right)\right]^{-1}, \tag{4.5}$$

and period

$$T = \frac{\sqrt{2}3^{\frac{1}{4}}K(\mu)}{Z\left(1-\rho+\rho^2\right)^{\frac{1}{4}}\sqrt{\cos\left(\frac{\alpha}{3}-\frac{\pi}{6}\right)}\sqrt{I_{13}}}, \tag{4.6}$$

where $K(\mu)$ is the complete elliptic integral of the first kind.

4.3 Solutions for amplitudes

We present explicit expressions for the amplitude squares. The convention used here is that the amplitudes are positive, which is the generic situation when $H_T \ne 0$. In this convention, when $H_T = 0$ the individual phases have discontinuities in time to account for the amplitudes' sign changes. The amplitude squares are proportional to the modes' energies and can be of great use for physical applications:

$$\begin{cases} C_1^2(t) = -\mu\left(\frac{2K(\mu)}{ZT}\right)^2 \mathbf{sn}^2\left(2K(\mu)\frac{(t-t_0)}{T},\mu\right)+\frac{I_{13}}{3}\left(2-\rho+2\sqrt{1-\rho+\rho^2}\cos\left(\frac{\alpha}{3}\right)\right), \\ C_2^2(t) = -\mu\left(\frac{2K(\mu)}{ZT}\right)^2 \mathbf{sn}^2\left(2K(\mu)\frac{(t-t_0)}{T},\mu\right)+\frac{I_{13}}{3}\left(2\rho-1+2\sqrt{1-\rho+\rho^2}\cos\left(\frac{\alpha}{3}\right)\right), \\ C_3^2(t) = \mu\left(\frac{2K(\mu)}{ZT}\right)^2 \mathbf{sn}^2\left(2K(\mu)\frac{(t-t_0)}{T},\mu\right)+\frac{I_{13}}{3}\left(\rho+1-2\sqrt{1-\rho+\rho^2}\cos\left(\frac{\alpha}{3}\right)\right), \end{cases} \tag{4.7}$$

where $\mathbf{sn}(\cdot,\mu)$ is Jacobian elliptic function and t_0 is given in terms of the initial conditions for the amplitudes $C_1^2(0)$, $C_2^2(0)$, $C_3^2(0)$ and t_0 is defined by the initial conditions as:

$$t_0 = \text{sign}(\cos\varphi(0))\frac{T}{2K(\mu)} \times F(\arcsin\sqrt{x_0},\mu), \tag{4.8}$$

where

$$x_0 = \frac{\cos\left(\dfrac{\alpha}{3}\right)}{\sqrt{3}\cos\left(\dfrac{\alpha}{3}+\dfrac{\pi}{6}\right)} + \frac{Z^2 T^2 (C_3^2(0) - C_2^2(0) - C_1^2(0))}{12\mu K(\mu)^2} \tag{4.9}$$

and $F(\cdot,\mu)$ is the elliptic integral of the first kind.

Notice that each equation in (4.7) is a sum of two terms where the left terms are time-dependent and the right terms are not. Each right term, for instance

$$\frac{I_{13}}{3}\left(2-\rho+2\sqrt{1-\rho+\rho^2}\cos\left(\frac{\alpha}{3}\right)\right)$$

can be written explicitly as a function of conserved quantities I_{13}, I_{23}, H_T (expressions for ρ and α are given by (4.3) and (4.4)) and is, therefore, defined by the initial conditions.

The same is true for μ and T as it follows from (4.5) and (4.6). In particular, one can use the equations in (4.7) to determine the minimum and maximum accessible values of each amplitude (using the fact that $\mathbf{sn}^2$ oscillates between 0 and 1). The characteristic energy variation of any resonant mode E_{mode}, between these minimum and maximum values, has a very simple form: $E_{mode}(t) \sim \mathbf{sn}^2(kt,\mu)$.

4.4   Solution for dynamical phase

The dynamical phase satisfies an evolution equation:

$$\dot{\varphi} = -ZH_T\left(C_1^{-2}+C_2^{-2}-C_3^{-2}\right). \tag{4.10}$$

The solution for the dynamical phase **cannot** be obtained by simply replacing the solution for the amplitudes in the Hamiltonian $H_T = C_1 C_2 C_3 \sin\varphi$ and solving for φ. The reason is that non-zero φ generically evolves between 0 and π, crossing the value $\varphi = \pi/2$ periodically. This implies that $\sin^{-1}$ is double-valued and thus it is not possible to obtain φ in a unique way.

Another way to obtain the solution for dynamical phase might be integrating (4.10) in time, using the solution for the amplitude squares (4.7), but this way is also rather involved. On the other hand, some simple considerations allow us to find an analytical expression for the dynamical phase. Indeed, let us rewrite (4.2), taking into account that $dC_1^2/dt = 2C_1\dot{C}_1$ and $H_T = C_1 C_2 C_3 \sin\varphi$:

$$\frac{d}{dt}C_1^2 = 2ZC_1 C_2 C_3 \cos\varphi = 2ZH_T\cot\varphi.$$

This equation can be solved for φ in each of the disjoint domains $(0,\pi)$ and $(-\pi,0)$:

$$\varphi(t) = \text{sign}(\varphi(0))\,\text{arccot}\left(\frac{\text{sign}(\varphi(0))\frac{d}{dt}C_1^2}{2ZH_T}\right),$$

using the convention that the function arccot takes values on $(0,\pi)$. Using solution (4.7) together with the identity $\mathbf{sn}'(x,\mu) = \mathbf{cn}(x,\mu)\mathbf{dn}(x,\mu)$, we arrive at an explicit expression for the dynamical phase:

$$\varphi(t) = \text{sign}(\varphi_0)\,\text{arccot}\left(-\frac{\mu}{|H_T|}\left(\frac{2K(\mu)}{ZT}\right)^3 y\right), \tag{4.11a}$$

$$y = \mathbf{sncndn}\left(2K(\mu)\frac{(t-t_0)}{T},\mu\right), \tag{4.11b}$$

where $\mathbf{sncndn}(\cdot,\mu) \equiv \mathbf{sn}(\cdot,\mu)\mathbf{cn}(\cdot,\mu)\mathbf{dn}(\cdot,\mu)$.

The restriction to the domain $\varphi \in (-\pi,0)\cup(0,\pi)$ is quite general: if φ is initially in the domain $(n\pi,(n+1)\pi)$, $n \in \mathbb{Z}$, one can take φ to either $(-\pi,0)$ or $(0,\pi)$ by an appropriate shift of $2m\pi, m \in \mathbb{Z}$, without changing the evolution equations. Due to its special dynamics, the phase will remain in the domain where it was initially.

4.5 Dynamical invariant

Below we present a dynamical invariant for (4.2) which has been used for the constructing the solution (4.7). Recall that a dynamical invariant depends on time, amplitudes and phases: $S(t,C_1,C_2,C_3,\varphi)$, with the property that it is a constant along any solution of the dynamical system. Generically, only local expressions can be obtained for a dynamical invariant, due to the multi-valuedness of the inverse functions involved. In this particular case, however, since we know the period of any trajectory, this multi-valuedness can be eliminated partially by patching appropriately local expressions yielding

$$S(t,C_1,C_2,C_3,\varphi) = t - \left\lfloor\frac{2(t-t_0)+T}{2T}\right\rfloor T + \frac{(-1)^{\left\lfloor\frac{2(t-t_0)+T}{T}\right\rfloor}T}{2K(\mu)}F(\arcsin\sqrt{x_t},\mu), \tag{4.12}$$

where $\lfloor \cdot \rfloor$ is the floor function and x_t can be obtained from the expression (4.9) for x_0 by substituting $C_j(t)$ instead of $C_j(0)$, for all $j=1,2,3$.

This dynamical invariant satisfies

$$S(t,C_1(t),C_2(t),C_3(t),\varphi(t)) = t_0, \quad \forall t,$$

where t_0 is given in Eq. (4.8), and is an improvement of the corresponding formula presented in [4].

In Fig. 6, we show, for fixed $I_{13} = 2.00$ and $I_{23} = 2.06$: level surface of conservation law $H_T = 0.763$ (Fig. 6(a)), level surface of dynamical invariant $S = 2.69$ (Fig. 6(b)), solution trajectory and combined plot, in the domain (C_1,φ,t) (Fig. 6(c) and (d) correspondingly).

(a)   (b)   (c)

(d)   (e)   (f)
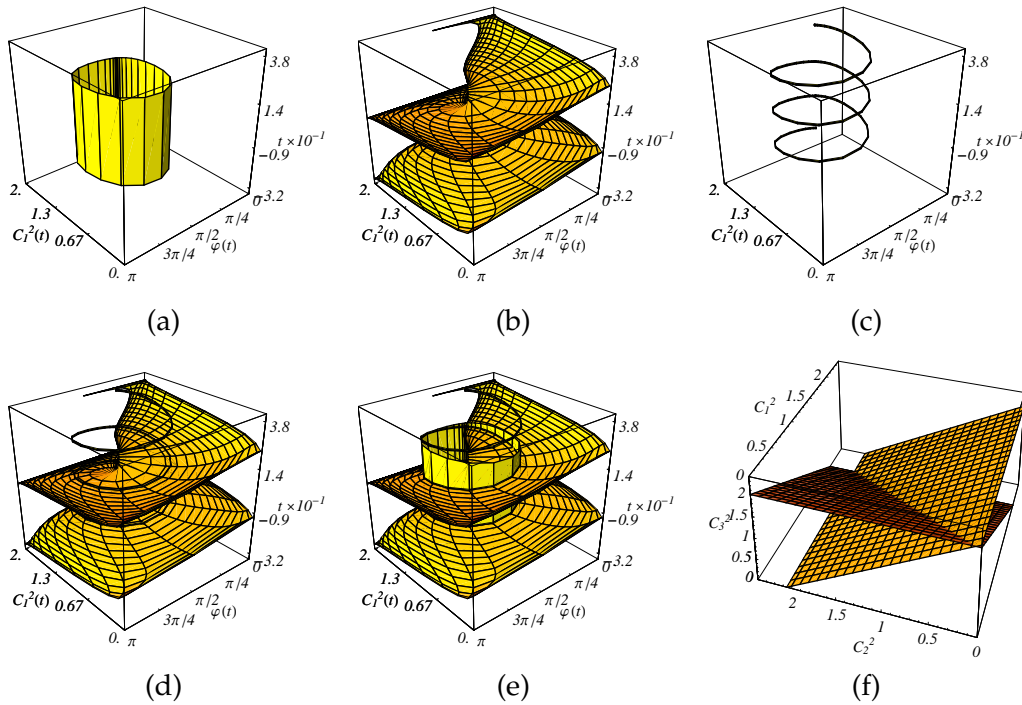
Figure 6: Color online. Triad system in coordinates (C_1^2, φ, t), with fixed values of the Manley-Rowe conservation laws: $I_{13} = 2.00$ and $I_{23} = 2.06$. (a): level surface of conservation law $H_T = 0.763$. (b): level surface of dynamical invariant $S = 2.69$, Eq. (4.12). (c): solution trajectory $(C_1^2(t), \varphi(t))$, Eqs. (4.7) and (4.11), corresponding to $H_T = 0.763$, $S = 2.69$. (d): combined plot of level surface of dynamical invariant $S = 2.69$ and solution trajectory $(C_1(t)^2, \varphi(t))$. (e): combined plot of level surface of conservation law $H_T = 0.763$, level surface of dynamical invariant $S = 2.69$ and solution trajectory $(C_1^2(t), \varphi(t))$. Notice the general property that the intersection of the level surfaces of H_T and S *is* the solution trajectory. (f): combined plot of Manley-Rowe conservation laws $I_{13} = 2.00$ and $I_{23} = 2.06$, in coordinates (C_1^2, C_2^2, C_3^2).
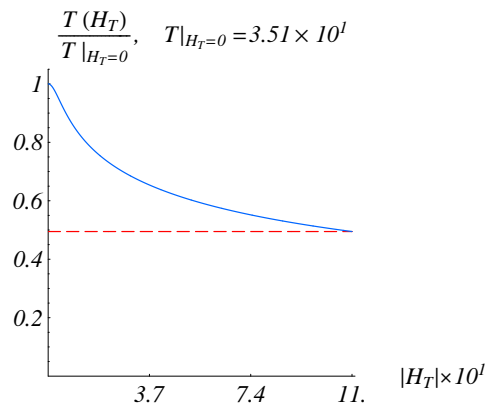
Figure 7: Color online. With fixed values of the Manley-Rowe conservation laws: $I_{13} = 2.00$ and $I_{23} = 2.06$, plot of period T from Eq. (4.6) as a function of H_T, normalized with respect to the period at $H_T = 0$. The decreasing character is a generic feature of this function.

In Fig. 6(a), the surface $S = 2.69$ is a helicoidal surface revolving around a vertical axis. This axis is the surface's natural interior boundary: the constant-in-time trajectory corresponding to the highest possible value of $|H_T|$ for given I_{13}, I_{23} (obtained from the condition $\cos\alpha = -1$). In the present case, the highest possible value of $|H_T|$ is 1.114. This trajectory is physically interpreted as "maximum interference", due to the fact that the modes do not interact. The dynamical phase is constant: $\varphi(t) = \pi/2$, $\forall t$, and all amplitudes are constant as well: from the condition $\mu = 0$ and Eq. (4.7), we obtain in this case: $C_1^2(t) = 1.33$, $\forall t$. The exterior boundary of the surface is the piecewise continuous trajectory corresponding to the limit $H_T = 0$: in this limit the surface becomes non-differentiable at the "corners" $C_1^2 = 0, I_{13}, \varphi = 0, \pi$, due to the fact that the dynamical phase φ is only piecewise continuous for $H_T = 0$. This trajectory corresponds to the usual case treated in textbooks, when amplitudes are considered real and individual phases vanish.

By looking at this figure we notice that the period T decreases with increasing H_T: the trajectories closer to the exterior boundary are more elongated than the trajectories closer to the interior boundary. In fact, from formula (4.6) one can prove this property analytically. In Fig. 7 we plot the period T as a function of H_T. We observe in this case a reduction of the period by a factor 0.5 when H_T is changed from 0 to $H_{\max} = 1.114$.

In Fig. 6(e) and (f), combined plots are shown to clarify that the solution trajectory is the intersection of the level surfaces of Hamiltonian and dynamical invariant. In the right lower panel, we show a combined plot of level surfaces of Manley-Rowe conservation laws I_{13}, I_{23} in the domain (C_1^2, C_2^2, C_3^2).

4.6 Special case $H_T = 0$

Direct substitution shows that if we put $H_T = 0$, then new modulus and period take the form

$$\mu = \rho \quad \text{and} \quad T = \frac{2K(\rho)}{Z\sqrt{I_{13}}},$$

correspondingly, while the solutions for the amplitude squares read

$$\begin{cases} \widetilde{C}_1^2(t) = \mathrm{dn}^2\big((t-t_0)Z\sqrt{I_{13}}, \rho\big) I_{13}, \\ \widetilde{C}_2^2(t) = \mathrm{cn}^2\big((t-t_0)Z\sqrt{I_{13}}, \rho\big) I_{23}, \\ \widetilde{C}_3^2(t) = \mathrm{sn}^2\big((t-t_0)Z\sqrt{I_{13}}, \rho\big) I_{23}. \end{cases} \tag{4.13}$$

As for the dynamical phase, from Eq. (4.11) it is seen that in the limit $H_T \to 0$ it behaves as a step function, jumping from 0 to $\pi \operatorname{sign}(\varphi(0))$:

$$\widetilde{\varphi}(t) = \frac{\pi \operatorname{sign}(\varphi(0))}{2}\left(1 - (-1)^{\left\lfloor \frac{2(t-t_0)}{T} \right\rfloor}\right).$$

To understand the meaning of this behaviour, notice that the Hamiltonian H_T is vanishing for $\varphi = n\pi$, $n \in \mathbb{Z}$. The abrupt jumps of the dynamical phase is due to the jumps of the

individual phases (solution not shown). These jumps replace the changes of sign of the modes' amplitudes in the usual textbook descriptions.

As it was shown in [5], initial dynamical phase not in $\mathbb{Z}\pi$ substantially affects the magnitudes of resonantly interacting modes during the evolution, not only in a triad but also in a butterfly. This fact might have important implications (see [5], Discussion), for instance, for interpreting results of numerical simulations and for performing laboratory experiments.

5   Generic clusters

In a three-wave resonance systems the most frequently met clusters are isolated triads or clusters consisting of two variously connected triads, e.g., [27, 29, 33, 35]. Below we show how to construct new CLs making use of the notion of dynamical invariant. In the last subsection, another method is briefly outlined which was presented in [66, 67] and allows one to prove, in some cases, integrability of bigger clusters.

5.1   Butterfly

A *PP-butterfly* consists of two triads *a* and *b* with wave amplitudes B_{ja}, B_{jb}, $j = 1,2,3$, and connecting mode, say $B_{1a} = B_{1b} = B_1$ is passive in both triads. The dynamical system for PP-butterfly reads

$$\begin{cases} \dot{B}_1 = Z_a B_{2a}^* B_{3a} + Z_b B_{2b}^* B_{3b}, & \dot{B}_{2a} = Z_a B_1^* B_{3a}, \\ \dot{B}_{2b} = Z_b B_1^* B_{3b}, & \dot{B}_{3a} = -Z_a B_1 B_{2a}, & \dot{B}_{3b} = -Z_b B_1 B_{2b}. \end{cases} \tag{5.1}$$

We have studied this in [4]; we present here the results in order to compare the dynamics of different butterfly types and confirm the qualitative analysis given in [33]. System (5.1) has 3 quadratic CLs analogous to (2.2) and 1 cubic CL corresponding to its Hamiltonian:

$$\begin{cases} I_{23a} = |B_{2a}|^2 + |B_{3a}|^2, & I_{23b} = |B_{2b}|^2 + |B_{3b}|^2, \\ I_{ab} = |B_1|^2 + |B_{3a}|^2 + |B_{3b}|^2, \\ H_{PP} = \mathrm{Im}(Z_a B_1 B_{2a} B_{3a}^* + Z_b B_1 B_{2b} B_{3b}^*). \end{cases} \tag{5.2}$$

Standard amplitude-phase representation. Here, one can rewrite the cubic conservation law as

$$H_{PP} = C_{PP}\left(Z_a C_{2a} C_{3a} \sin\varphi_a + Z_b C_{2b} C_{3b} \sin\varphi_b\right). \tag{5.3}$$

Here

$$\varphi_a = \theta_{1a} + \theta_{2a} - \theta_{3a}, \qquad \varphi_b = \theta_{1b} + \theta_{2b} - \theta_{3b} \tag{5.4}$$

are dynamical phases and $C_{(PP)}$ is the real amplitude of a common mode in PP-butterfly. This allows us to reduce System (5.1) to only four real equations:

$$\begin{cases} \dot{C}_{3a} = -Z_a C_{PP} C_{2a} \cos\varphi_a, & \dot{C}_{3b} = -Z_b C_{PP} C_{2b} \cos\varphi_b, \\ \dot{\varphi}_a = -H_{PP}(C_{PP}^{-2} + C_{2a}^{-2} - C_{3a}^{-2}), & \dot{\varphi}_b = -H_{PP}(C_{PP}^{-2} + C_{2b}^{-2} - C_{3b}^{-2}). \end{cases}$$ (5.5)

Now the overall dynamics of the PP-butterfly is confined to a 3-dimensional manifold. The same can be done for the two other types of butterflies.

Modified amplitude-phase representation. The following change of variables was suggested in [4]:

$$\alpha_a = \arctan\left(\frac{C_{3a}}{C_{2a}}\right), \qquad \alpha_b = \arctan\left(\frac{C_{3b}}{C_{2b}}\right),$$ (5.6)

with the inverse transformation being

$$\begin{cases} C_{2a} = \sqrt{I_{23a}}\cos\alpha_a, & C_{3a} = \sqrt{I_{23a}}\sin\alpha_a, \\ C_{2b} = \sqrt{I_{23b}}\cos\alpha_b, & C_{3b} = \sqrt{I_{23b}}\sin\alpha_b. \end{cases}$$ (5.7)

This change of variables allows further substantial simplification of (5.1) and (5.5):

$$\begin{cases} \dot{\alpha}_a = -Z_a C_{PP}\cos\varphi_a, & \dot{\alpha}_b = -Z_b C_{PP}\cos\varphi_b, \\ \dot{\varphi}_a = Z_a C_{PP}(\cot\alpha_a - \tan\alpha_a)\sin\varphi_a - H_{PP}/C_{PP}^2, \\ \dot{\varphi}_b = Z_b C_{PP}(\cot\alpha_b - \tan\alpha_b)\sin\varphi_b - H_{PP}/C_{PP}^2. \end{cases}$$ (5.8)

In these new variables, the amplitude $C_{PP} > 0$ reads

$$C_{PP} = \sqrt{I_{ab} - I_{23a}\sin^2\alpha_a - I_{23b}\sin^2\alpha_b}$$ (5.9)

and the Hamiltonian is now

$$H_{PP} = \frac{C_{PP}}{2}Z_a I_{23a}\sin\varphi_a\sin2\alpha_a + \frac{C_{PP}}{2}Z_b I_{23b}\sin\varphi_b\sin2\alpha_b.$$ (5.10)

Eqs. (5.8)-(5.10) represent the final form of our three-dimensional general system in the modified amplitude-phase presentation.

Of course, the form of the conservation laws is arbitrary in the sense that any set of functionally independent CLs will be suitable. For instance, in the case $H_{PP} = 0$ we could choose the conserved quantity

$$A_b = \sin\varphi_b\sin2\alpha_b \text{ instead of } A_a = \sin\varphi_a\sin2\alpha_a$$

but not both because they are functionally dependent:

$$Z_a I_{23a} A_a + Z_b I_{23b} A_b \equiv 0.$$

Figure 8: NR-diagram for PP-butterfly.

Figure 9: NR-diagram for AA-butterfly.

Generally, we try to find the simplest presentation for our new constants of motion.

Analogously with the previous case, *AA-butterfly* is a two-triad cluster with a common mode which is A-mode in both triads, $B_{3a} = B_{3b}$. Dynamical system and Manley-Rowe constants read:

$$\begin{cases} \dot{B}_{1a} = Z_a B_{2a}^* B_{3a}, & \dot{B}_{1b} = -Z_b B_{2b}^* B_{3a}, & \dot{B}_{2a} = Z_a B_{1a}^* B_{3a}, \\ \dot{B}_{2b} = Z_b B_{1b}^* B_{3a}, & \dot{B}_{3a} = -Z_a B_{1a} B_{2a} - Z_b B_{1b} B_{2b}, \end{cases} \tag{5.11}$$

$$I_{12a} = |B_{1a}|^2 - |B_{2a}|^2, \quad I_{12b} = |B_{1b}|^2 - |B_{2b}|^2, \quad I_{ab} = |B_{1a}|^2 + |B_{3a}|^2 + |B_{3b}|^2. \tag{5.12}$$

The integrability of (5.11) can be investigated along the same lines as for (5.1) above. The analysis is omitted here. We just partly outline one particular case of this cluster: AA-ray, which can be regarded as a degenerate AA-butterfly, so that $\omega_{1b} = \omega_{2b} = \omega_3 / 2$. In this case, the dynamical system obtained from first principles will have the form

$$\dot{B}_{1a} = Z_a B_{2a}^* B_3, \quad \dot{B}_b = Z_b B_b^* B_3, \quad \dot{B}_{2a} = Z_a B_{1a}^* B_3, \quad \dot{B}_3 = -Z_a B_{1a} B_{2a} - 2 Z_b B_b^2. \tag{5.13}$$

Notice that there is a factor 2 in the last term of last equation, which would not appear if we made the direct substitution $B_{1b} = B_{2b} = B_b$ into system (5.11). Rather, the simple change of variables $B_{1b} = B_{2b} = \sqrt{2} B_b$ will transform the AA-butterfly (5.11) into the ray equations (5.13). This means in particular that integrable cases of AA-butterfly can be directly mapped to some integrable cases of AA-ray. Another interesting point is that AA-ray cluster might also have a nice mechanical model-Wilberforce pendulum (P. Lynch, private communication, 2009).

Conservation laws for AA-ray are inherited from conservation laws for AA-butterfly:

$$I_{12a} = |B_{1a}|^2 - |B_{2a}|^2, \quad I_{ab} = |B_{1a}|^2 + 2|B_b|^2 + |B_3|^2, \tag{5.14a}$$

$$H_{\text{ray}} = \text{Im}(-Z_a B_{1a} B_{2a} B_3^* - 2 Z_b B_b^2 B_3^*), \tag{5.14b}$$

with dynamical phases

$$\varphi_a = \theta_{1a} + \theta_{2a} - \theta_3, \qquad \varphi_b = 2\theta_b - \theta_3. \tag{5.15}$$

This reduces four complex equations (5.13) to only four real ones:

$$
\begin{cases}
\dot{C}_{1a} = Z_a C_{2a} C_3 \cos\varphi_a, \quad \dot{C}_b = Z_b C_b C_3 \cos\varphi_b, \\
\dot{\varphi}_a = -Z_a C_3 \left(\dfrac{C_{2a}}{C_{1a}} + \dfrac{C_{1a}}{C_{2a}} \right) \sin\varphi_a + H_{\mathrm{ray}}/C_3^2, \\
\dot{\varphi}_b = -2 Z_b C_3 \sin\varphi_b + H_{\mathrm{ray}}/C_3^2,
\end{cases}
\tag{5.16}
$$

with Hamiltonian

$$
H_{\mathrm{ray}} = -C_3 \left(Z_a C_{1a} C_{2a} \sin\varphi_a + 2 Z_b C_b^2 \sin\varphi_b \right)
\tag{5.17}
$$

in terms of the amplitudes and phases.

Consider the simple case when initially $\varphi_a = \varphi_b = 0$. Then $H_{\mathrm{ray}} = 0$, phases remain zero for all times, and the equations of motion reduce to

$$
\dot{C}_{1a} = Z_a C_{2a} C_3, \quad \dot{C}_{2a} = Z_a C_{1a} C_3, \quad \dot{C}_b = Z_b C_b C_3, \quad \dot{C}_3 = -Z_a C_{1a} C_{2a} - 2 Z_b C_b^2,
\tag{5.18}
$$

with two Manley-Rowe constants of motion

$$
I_{12a} = C_{1a}^2 - C_{2a}^2, \qquad I_{ab} = C_{1a}^2 + 2 C_b^2 + C_3^2,
\tag{5.19}
$$

and a new Hamiltonian

$$
H_{\mathrm{new}} = 2 Z_a \ln C_b + Z_b \ln\left(\frac{C_{2a} - C_{1a}}{C_{2a} + C_{1a}} \right),
\tag{5.20a}
$$

$$
C_{1a} = \sqrt{I_{12a}} \cosh\alpha, \qquad C_{2a} = \sqrt{I_{12a}} \sinh\alpha.
\tag{5.20b}
$$

5.2 Star

A cluster of N triads, all connected *via* one common mode is called N-star cluster. Again, integrability of N-star depends on the types these connecting modes have in each triad of a cluster. NR-diagrams for all possible types of 3-stars are shown in Fig. 10. N-star cluster is the only known to us type of cluster for which an analytical study has been performed for *arbitrary* finite number N. The main idea can be briefly formulated as follows. N-star cluster has $2N+1$ degrees of freedom, $N+1$ Manley-Rowe constants of motion and one Hamiltonian, that is, we already have $N+2$ independent first integrals in involution. To find $N-1$ additional integrals of motion, one can use construction of Lax operators, Painlevé analysis and irreducible forms, etc.; terminology used therein is pump and daughter wave for A- and P-mode correspondingly). The dynamical system, say for N-star-A, is regarded in the form

$$
\dot{B}_{1j} = i \lambda_j B_3 \dot{B}_{2j}, \qquad \dot{B}_{2j} = i \lambda_j B_3 \dot{B}_{1j}, \qquad \dot{B}_3 = i \sum_{j=1}^{N} \lambda_j B_{1j} B_{2j}.
\tag{5.21}
$$
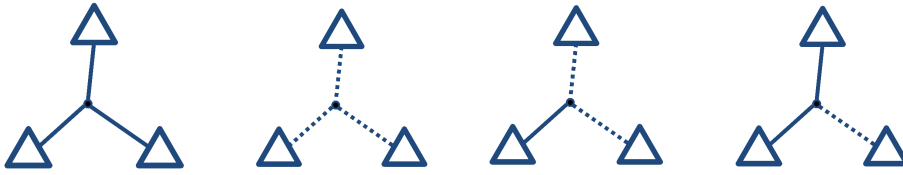
Figure 10: NR-diagrams for 3-star clusters. From right to left, from up to down: 3-star-A (three A-connections), 3-star-P (three P-connections), 3-star-1A-2P (one P-connection and two P-connections), 3-star-2A-1P (two A-connections and one P-connection).
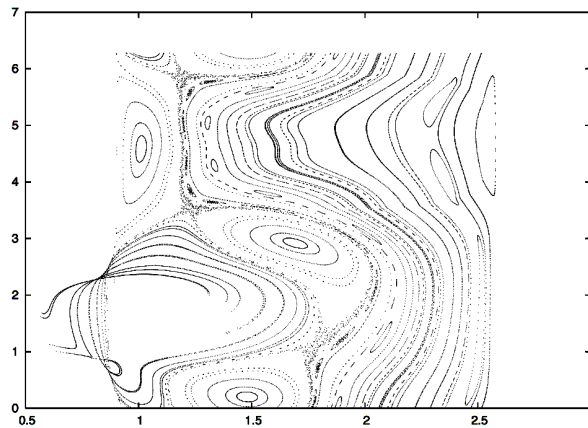
Figure 11: Example of Poincaré section for PP-butterfly with $Z_a/Z_b = 3/4$.

Additional conservation laws found this way have necessarily *polynomial form*. The results for a generic N-star cluster are as follows: N-star-A (with all A-connections) and N-star-P (with all P-connections) are integrable for *arbitrary initial conditions* if $\lambda_j = 1/2$ or 1 or 2, examples of corresponding NR-diagrams shown in the Fig. 10, for $N = 3$. N-star cluster with mixed P- and P-connections has no additional polynomial conservation laws. Complete set of additional polynomial conservation laws for integrable N-star cluster is omitted here for sake of place, and it can be found in [67]. Example for the case of AA-butterfly with $Z_a = 2Z_b$ reads

$$4(B_1 B_2 B_4^* B_5^* + B_1^* B_2^* B_4 B_5)(B_1 B_1^* + B_2 B_2^*) - 2(B_3 B_1^* B_2^* + B_3^* B_1 B_2)^2$$
$$- \left[(B_1 B_1^* + B_2 B_2^*)^2 + 4 B_1 B_1^* B_2 B_2^* \right] (B_4 B_4^* + B_5 B_5^*).$$

However, most generic clusters demonstrate chaotic behavior and numerical investigations are unavoidable. The fact that our systems are Hamiltonian, allows us to perform numerical simulations based on the Hamiltonian expansion of the corresponding dynamical system and to construct Poincaré sections, example is in shown in the Fig. 11 (chaotic evolution, simulations performed by F. Leyvraz 2008).

6   Coupling coefficient

As we have shown above, the integrability of a resonance cluster depends on the magnitude of the corresponding coupling coefficients. Expressions for coupling coefficients in *canonical variables* has been deduced for various types of wave systems possessing three-wave resonances: rotational capillary waves [10]; irrotational gravity-capillary waves [47]; drift waves [60], etc. They usually have a nice compact form, for instance, coupling coefficient V_{12}^3 for irrotational gravity-capillary water waves reads

$$\frac{(\omega_2^2 - \omega_2\omega_3 + \omega_3^2)}{\omega_1}k_1 - \omega_2 k_2 + \omega_3 k_3,$$

where $\omega = (gk + \sigma k^3)^{1/2}$ and g and σ are gravity acceleration and surface tension correspondingly. However, transformation of these expressions from the canonical to *physical variables* is not an easy task.

On the other hand, the application of multi-scale methods yields expressions for the coupling coefficients directly in physical variables. For instance, coupling coefficients of the system of three resonantly interacting atmospheric planetary waves, with $\omega \sim m/[n(n+1)]$, have the form [35]

$$Z[n_2(n_2+1) - n_3(n_3+1)][n_1(n_1+1)]^{-1}, \tag{6.1a}$$

$$Z[n_3(n_3+1) - n_1(n_1+1)][n_2(n_2+1)]^{-1}, \tag{6.1b}$$

$$Z[n_2(n_2+1) - n_1(n_1+1)][n_3(n_3+1)]^{-1}, \tag{6.1c}$$

with

$$Z = \int_{-\frac{\pi}{2}}^{\frac{\pi}{2}} \left[m_2 P^{(2)}\frac{d}{d\varphi}P^{(1)} - m_1 P^{(1)}\frac{d}{d\varphi}P^{(2)} \right] \frac{d}{d\varphi}P^{(3)}d\varphi. \tag{6.2}$$

Here two spherical space variables are the latitude φ, $-\pi/2 \le \varphi \le \pi/2$, and the longitude λ, $0 \le \lambda \le 2\pi$, and the notation $P^{(j)}$ is used for $P_{n_j}^{m_j}(\sin\varphi)$ which is the associated Legendre function of degree n_j and order m_j.

The multi-scale method is quite straightforward and can be programmed in some symbolical language [35]. However, only numerical magnitudes of the coupling coefficients have been computed for selected solutions of the resonance conditions, not an explicit algebraic formulas. The problem is due to some "bags" in *Mathematica* in computing integrals of the form

$$\int_0^{2\pi} \sin(mx)\sin(nx)dx, \quad \text{with } m,n \in \mathbb{N}, \tag{6.3}$$

more discussion can be found in [35].

7 Summary

In this review we presented analytical methods and available results for studying resonance clustering in discrete and mesoscopic wave turbulent regimes. Some resonance clusters can generate regular patterns (elements of integrability in the terminology of F. Calogero) in k-space. The clusters can also demonstrate chaotic behavior depending on the form its NR-diagram, ratios of coupling coefficients and in some cases-on the initial conditions. Both type of cluster-with integrable and chaotic dynamics-do appear in real physical systems, e.g., [32,33] and [9] (atmospheric planetary and rotational capillary waves correspondingly).

In particular, the novel model of the intra-seasonal oscillations (climate variability on an intra-seasonal scale of about 10-100 days) in the Earth's atmosphere has been developed in [32], based on the corresponding resonance clustering. A detailed analysis of the classical approach to the problem can be found in [15]. However, it does not explain many known features of the intra-seasonal oscillations (IOs): e.g., the reason for their appearance in the Northern Hemisphere is supposed to be topography, no reason is given for IOs in the Southern Hemisphere, there is no known way to predict the appearance of IOs, etc. The resonance clustering in the form of four isolated resonant triads gives a natural explanation of IOs in both the Northern and the Southern Hemispheres, independently (in the leading order) of Earth's topography. It naturally has the periods of desired order, and allows one to interpret the main observable features of IOs as an intrinsic atmospheric phenomenon, related to a system of resonantly interacting triads of planetary waves.

To describe resonance clustering in a specific wave system one has to proceed as follows: 1) write out the resonance conditions, compute their solutions and construct corresponding set of NR-diagrams; 2) write out explicitly the set of dynamical systems, interaction coefficient and known conservation laws, according to the clustering. Corresponding software (written in Mathematica, Java, SQL and C++) is described in [28,35], some of the programs are available for free download for on-line computations, an electronic supplement for the last book.

The study of the dynamical systems can be performed afterwards using analytical and/or numerical methods. While performing sensible numerical simulations with dynamical system describing a resonance cluster, one of the most tedious and time-consuming parts of the corresponding simulations is the choice of initial conditions. A special procedure has been worked out (F. Leyvraz, 2008) that guarantees a uniform distribution of initial conditions according to Liouville measure, and assures as well that all conservation laws have the same value on each Poincaré section (example of computations in shown in Fig. 11). However, to trace effects due to the dynamical phases one has to amplitude-phase representations.

Last but not least. As it was mentioned before, the importance of resonance clusters is due to the fact that in a system possessing resonances, all non-resonant terms can be eliminated by suitable change of variables. It implies that the energies of interacting

modes are *bounded*. However, in some physical systems non-resonant terms can be of importance while they might provide *unbounded* solutions. This phenomenon is called explosive instability and has been discovered in plasma physics in 1960s-1970s. Conditions for this phenomenon to occur are known, both in 3- and 4-wave systems. This subject is outside the scope of present paper, its detailed exposition (state of art 1986) can be found e.g., in [57]; contemporary results on the explosive instability are briefly outlined in [28], 117–122.

Acknowledgments

References

[1] F. Almonte, V. K. Jirsa, E. W. Large and B. Tuller, Integration and segregation in auditory streaming, Phys. D, 212(1-2) (2005), 137–159.

[2] V. I. Arnold, Geometrical Methods in the Theory of Ordinary Differential Equations, Grundleheren der mathematischen Wissenschaften 250, A Series of Comprehensive Studies in Mathematics, New York Heidelberg Berlin, Springer-Verlag, 1983.

[3] A. V. Bolsino and A. T. Fomenko, Integrable Hamiltonian Systems, Chapmann & Hall/CRC, 2004.

[4] M. D. Bustamante and E. Kartashova, Dynamics of nonlinear resonances in Hamiltonian systems, Europhys. Lett., 85 (2009), 14004-1–14004-5.

[5] M. D. Bustamante and E. Kartashova, Effect of the dynamical phases on the nonlinear amplitudes' evolution, Europhys. Lett., 85 (2009), 34002-1–34002-6.

[6] F. Calogero, Why are certain nonlinear PDEs both widely applicapable and intergable? in book: V. E. Zakharov (ed.), What is Integrability?, 1 (1991), 1–62, Springer Series in Nonlinear Dynamics, Springer Verlag.

[7] C. C. Chow, D. Henderson and H. Segur, A generalized stability criterion for resonant triad interactions, Fluid Mech., 319 (1996), 67–76.

[8] B. Cretin and D. Vernier, Quantized amplitudes in a nonlinear resonant electrical circuit, E-print: arxiv.org/abs/0801.1301 (2008).

[9] A. Constantin and E. Kartashova, Effect of non-zero constant vorticity on the nonlinear resonances of capillary water waves, Europhys. Lett., 86 (2009), 29001-1–29001-6.

[10] A. Constantin, E. Kartashova and E. Wahlén, Discrete wave turbulence of rotational capillary water waves, E-print: arXiv:1001.1497 (2010).

[11] P. Denissenko, S. Lukaschuk and S. Nazarenko, Gravity surface wave turbulence in a laboratory flume, Phys. Rev. Lett., 99 (2007), 014501-1–014501-4.

[12] B. Dubrovin and Y. Zhang, Normal forms of hierarchies of integrable PDEs, Frobenius manifolds and Gromov-Witten invariants, E-print: arXiv:math/0108160v1 (2001).

[13] M. Eissa, W. A. A. El-Ganainia and Y. S. Hameda, Saturation, stability and resonance of non-linear systems, Phys. A: Stat. Mech. Appl., 356(2-4) (2005), 341–358.

[14] N. W. Evans, Superintegrability in classical mechanics, Phys. Rev. A, 41(10) (1990), 5666–5676.

[15] M. Ghil, D. Kondrashov, F. Lott and A. W. Robertson, Intraseasonal oscillations in the mid-latitudes: observations, theory, and GCM results, in: Proc. ECMWF/CLIVAR Workshop on Simulations and prediction of Intra-Seasonal Variability, Reading, UK, 2004.

[16] P. Haenggi, Stochastic resonance in biology how noise can enhance detection of weak signals and help improve biological information processing, ChemPhysChem, 3(3) (2002), 285–290.

[17] K. Hasselmann, A criterion for nonlinear wave stability, Fluid Mech., 30 (1967), 737–739.

[18] K. Horvat, M. Miskovic and O. Kuljaca, Avoidance of nonlinear resonance jump in turbine governor positioning system using fuzzy controller, Industrial Technology, 2 (2003), 881–885.

[19] R. S. Johnson, A Modern Introduction to the Mathematical Theory of Water Waves, Cambridge University Press, 1997.

[20] E. A. Kartashova, L. I. Piterbarg and G. M. Reznik, Weakly nonlinear interactions between Rossby waves on a sphere, Oceanology, 29 (1990), 405–411.

[21] E. Kartashova, Partitioning of ensembles of weakly interacting dispersing waves in resonators into disjoint classes, Phys. D, 46 (1990), 43–56.

[22] E. Kartashova, Weakly nonlinear theory of finite-size effects in resonators, Phys. Rev. Lett., 72 (1994), 2013–2016.

[23] E. Kartashova, Wave resonances in systems with discrete spectra, in book: Nonlinear Waves and Weak Turbulence, ed., Zakharov V. E. Series: Advances in the MathematicalSciences, AMS Transl., 2 (1998), 95–129.

[24] E. Kartashova, A model of laminated turbulence, JETP Lett., 83(7) (2006), 341–345.

[25] E. Kartashova, Fast computation algorithm for discrete resonances among gravity waves, Low Temp. Phys., 145(1-4) (2006), 286–295.

[26] E. Kartashova, Exact and quasi-resonances in discrete water-wave turbulence, Phys. Rev. Lett., 98(21) (2007), 214502-1–214502-4.

[27] E. Kartashova, Discrete wave turbulence, Europhys. Lett., 87 (2009), 44001-1–44001-6.

[28] E. Kartashova, Nonlinear Resonance Analysis: Theory, Computation, Applications, Cambridge University Press, 2010.

[29] E. Kartashova and A. Kartashov, Laminated wave turbulence: generic algorithms I, Int. J. Mod. Phys. C, 17(11) (2006), 1579–1596.

[30] E. Kartashova and A. Kartashov, Laminated wave turbulence: generic algorithms II, Commun. Comput. Phys., 2(4) (2007), 783–794.

[31] E. Kartashova and A. Kartashov, Laminated wave turbulence: generic algorithms III, Phys. A: Stat. Mech. Appl., 380 (2007), 66-74.

[32] E. Kartashova and V. S. L'vov, A model of intra-seasonal oscillations in the Earth atmosphere, Phys. Rev. Lett., 98(19) (2007), 198501-1–198501-4.

[33] E. Kartashova and V. S. L'vov, Cluster dynamics of planetary waves, Europhys. Lett., 83

(2008), 50012-1–50012-6.

[34] E. Kartashova and G. Mayrhofer, Cluster formation in mesoscopic systems, Phys. A: Stat. Mech. Appl., 385 (2007), 527–542.

[35] E. Kartashova, C. Raab, Ch. Feurer, G. Mayrhofer and W. Schreiner, Symbolic computations for nonlinear wave resonances, in: Extreme Ocean Waves: 97–128, Eds: E. Pelinovsky and Ch. Harif, Springer, 2008.

[36] E. Kartashova and A. Shabat, Computable Integrability, Chapter 1: General notions and ideas, RISC Report Series, N0002-04-2005, 2005.

[37] A. L. Karuzskii, A. N. Lykov, A. V. Perestoronin and A. I. Golovashkin, Microwave nonlinear resonance incorporating the helium heating effect in superconducting microstrip resonators, Phys. C: Superconduct., 408-410 (2004), 739–740.

[38] D. A. Kovriguine and G. A. Maugin, Multiwave nonlinear couplings in elastic structures, Math. Prob. Eng., doi:10.1155/MPE/2006/76041, 2006.

[39] M. Kundu and D. Bauer, Nonlinear resonance absorption in the laser-cluster interaction, Phys. Rev. Lett., 96 (2006), 123401-1–123401-4.

[40] F. Leyvraz, personal communication, 2008.

[41] M. S. Longuet-Higgins and A. E. Gill, Resonant interactions between planetary waves, Proc. Roy. Soc. Lond., A299 (1967), 120–140.

[42] V. S. L'vov, A. Pomyalov, I. Procaccia and O. Rudenko, Finite-dimensional turbulence of planetary waves, Phys. Rev. E, 80 (2009), 066319–43.

[43] P. Lynch, Resonant motions of the three-dimensional elastic pendulum, Int. J. Nonlinear Mech., 37 (2002), 258–264.

[44] P. Lynch, The swinging spring: a simple model of amospheric balance, in book: Large-Scale Atmosphere-Ocean Dynamics: Vol II: Geometric Methods and Models: 64–108, Eds. J. Norbury and I. Roulstone, Cambridge University Press, 2002.

[45] P. Lynch, private communication, 2009.

[46] P. Lynch and C. Houghton, Pulsation and pecession of the resonant swinging spring, Phys. D, 190 (2004), 38–62.

[47] L. F. McGoldrick, Resonant interactions among capillary-gravity waves, Fluid Mech., 21 (1967), 305–331.

[48] C. R. Menyuk, H. H. Chen and Y. C. Lee, Restricted multiple three-wave interactions: Panlevé analysis, Phys. Rev. A, 27 (1983), 1597–1611.

[49] C. R. Menyuk, H. H. Chen and Y. C. Lee, Restricted multiple three-wave interactions: integrable cases of this system and other related systems, J. Math. Phys., 24 (1983), 1073–1079.

[50] A. V. Mikhailov, A. B. Shabat and V. V. Sokolov, The symmetry approach to classification of integrable equations, in book: What is integrability?, 115, Ed. V. E. Zakharov, Springer Series in Nonlinear Dynamics, Springer Verlag, 1991.

[51] J. Moser, On invariant curves of area preserving mappings of an annulus, Nachr. Akad. Wiss. Goett, Math. Phys. Kl., 1 (1962), 1–20.

[52] J. Murdock, Normal Forms and Unfoldings for Local Dynamical Systems, Springer-Verlag, New York, 2003.

[53] S. L. Musher, A. M. Rubenchik and V. E. Zakharov, Hamiltonian approach to the description of nonlinear plasma phenomena, Phys. Rep., 129 (1985), 285–366.

[54] A. H. Nayfeh, Method of Normal Forms, Wiley-Interscience, NY, 1993.

[55] H. P. de Oliveira, I. Damia o Soares and E. V. Tonini, Nonlinear resonance of Kolmogorov-Arnold-Moser tori in bouncing universes, Cosmology and Astroparticle Physics, doi: 10.1088/1475-7516/2006/02/015, 2006.

[56] P. J. Olver, Applications of Lie groups to differential equations, Graduated Texts in Mathematics, 107, Springer, 1993.

[57] L. A. Ostrovskii, S. A. Rybak and S. L. Tsimring, Negative energy waves in hydrodynamics, Sov. Phys. Uspekhi., 29(11) (1986), 1040–1052.

[58] J. Pedlosky, Geophysical Fluid Dynamics, Second Edition, Springer, 1987.

[59] O. M. Phillips, On the dynamics of unsteady gravity waves of infinite amplitude, Fluid Mech., 9 (1960), 193–217.

[60] L. I. Piterbarg, Hamiltonian formalism for Rossby waves, AMS Trans., 2 (1998), 131–166.

[61] H. Punzmann, M. G. Shats and H. Xia, Phase randomization of three-wave interactions in capillary waves, Phys. Rev. Lett., 103 (2009), 064502-1–064502-4.

[62] A. N. Pushkarev, On the Kolmogorov and frozen turbulence in numerical simulation of capillary waves, Euro. J. Mech. B: Fluids, 18(3) (1999), 345–351.

[63] V. E. Syvokon, Yu. Z. Kovdrya and K. A. Nasyedkin, Nonlinear features of phonon-ripplon modes in the electron crystal over liquid Helium, Low Temp. Phys., 144(1-3) (2006), 35–48.

[64] R. Treumann and W. Baumjohann, Advanced Space Plasma Physics, Imperial Colledge Press, London, 2001.

[65] V. N. Tsytovich, Nonlinear effects in plasma, Plenum, New York, 1970.

[66] F. Verheest, Proof of integrability for five-wave interaactions in a case with unequal coupling constants, J. Phys. A: Math. Gen., 21 (1988), L545–L549.

[67] F. Verheest, Integrability of restricted multiple three-wave interactions II, coupling constants with ratios 1 and 2, J. Math. Phys., 29 (1988), 2197–2201.

[68] E. T. Whittaker and G. N. Watson, A Course in Modern Analysis, 4th ed., Cambridge, England, Cambridge University Press, 1990.

[69] W. B. Wright, R. Budakian and S. J. Putterman, Diffusing light photography of fully developed isotropic ripple turbulence, Phys. Rev. Lett., 76 (1996), 4528–4531.

[70] V. E. Zakharov, V. S. Lvov and G. Falkovich, Kolmogorov Spectra of Turbulence, Springer-Verlag, Berlin, 1992.

[71] V. E. Zakharov, Statistical theory of gravity and capillary waves on the surface of a finite-depth fluid, Euro. J. Mech. B: Fluids, 18 (1999), 327–344.

[72] V. E. Zakharov, Stability of periodic waves of finite amplitude on the surface of deep fluid, Zh. Prikl. Mekh. Tekh. Fiz., 9 (1968), 86–94.

[73] V. E. Zakharov and N.N. Filonenko, Weak turbulence of capillary waves, Appl. Mech. Tech. Phys., 4 (1967), 500–515.

[74] V. E. Zakharov, A. O. Korotkevich, A. N. Pushkarev and A. I. Dyachenko, Mesoscopic wave turbulence, JETP Lett., 82 (2005), 487–491.

[75] V. E. Zakharov and E. I. Shulman, Integrability of nonlinear systems and perturbation theory, in book: What is Integrability? Ed. V. E. Zakharov, Springer, 185, 1990.